Advances in Water Resources 32 (2009) 1465–1481

Contents lists available at ScienceDirect

Advances in Water Resources

journal homepage: www.elsevier.com/locate/advwatres

Analytical model of seasonal climate impacts on snow hydrology: Continuous snowpacks

Ross A. Woods *

National Institute for Water and Atmospheric Research (NIWA), 10 Kyle Street, Riccarton, Christchurch, New Zealand

ARTICLE INFO

Article history:
Received 11 July 2008
Received in revised form 25 June 2009
Accepted 28 June 2009
Available online 1 July 2009

Keywords:
Snow
Model
Seasonal
Climate
Analytical

ABSTRACT

We formulate and solve an analytical model of seasonal snowpack dynamics, by assuming a simple temperature index model for the snowpack, driven by purely seasonal climate forcing. Three dimensionless variables control the modeled system: one to indicate the temperature regime, one for the seasonality of both temperature and precipitation, and one for the mean precipitation rate relative to a characteristic melt rate. The purpose of the model is to provide insight into the relative roles of the mean and seasonality of temperature, the mean and seasonality of precipitation, and the melt factor, in controlling snow climatology.

The model can be used to make broad-scale predictions of the climatology of seasonal snow water storage, and its sensitivity to climate. Particular variables of interest include the maximum seasonal snow storage, the start and end of the snow accumulation period, and the time of year at which the snowpack is completely melted. The model makes useful uncalibrated predictions at six widely separated sites in the western USA which have a continuous seasonal snowpack.

The connections between the model and a widely-used snow classification of Sturm et al. are briefly explored. Limitations of the model are discussed, extensions to the model are foreshadowed, and an example is given of a global application. If further testing demonstrates that the model gives adequate estimates of seasonal snowpack response for a wider range of locations, we might envisage applications of this approach to (i) definition of hydrological similarity indices in snow-dominated regions (ii) interpretation of output from complex simulation models covering a wide range of environments (iii) screening-level analyses of sensitivity to climate variations (iv) low-dimensional modeling where there are limited data or computation resources or technical expertise.

1. Introduction

The seasonal development and depletion of snow cover is a visible and widespread feature of large areas of the earth's surface. Snow plays a major role in the terrestrial water and energy balance especially in the northern hemisphere, with major climatic, economic, ecological and cultural significance. The water stored in the snowpack can be a significant component of the hydrological cycle, and the magnitude and timing of this storage is sensitive to climate variability. The hydrological impacts of snow vary from having no effect at all in warm climates, to storing a large fraction of the annual precipitation as snow and then releasing it as snowmelt each year. This water storage is especially significant in cool climates with a winter maximum in precipitation.

There are many subtleties and local variations on this simple description, and as a consequence, quantitative hydrological intercomparison between snow-affected sites in different locations is difficult. Comparison may be relatively straightforward to do within a limited geographic region, on the basis of a single factor such as elevation or temperature. Such simple methods rely on other factors not varying significantly. The analysis presented in this paper allows for consideration of simultaneous variation in multiple factors, and the identification of controlling factors ("first order controls").

For example consider two contrasting sites where the seasonal temperature falls below zero for part of the year. One site is relatively cold and dry; the other is warmer and wetter. Which one has the longer snow season? Which one has the deeper seasonal snowpack? Can we give a compact quantitative explanation of the interactions between temperature and precipitation that are relevant to seasonal snowpack dynamics?

The interactions between atmospheric forcing and land surface processes in snow-dominated systems are complex and much remains to be quantified, especially for processes which are difficult to measure directly. However, enough is known to attempt a simplified synthesis of the controls on snow water equivalent. The general approach taken here is to define simplistic forcing and

* Tel.: +64 3 343 7803.
E-mail address: r.woods@niwa.co.nz

0309-1708/$ - see front matter © 2009 Elsevier Ltd. All rights reserved.
doi:10.1016/j.advwatres.2009.06.011

dynamics, in order to identify dimensionless similarity variables which define the system dynamics at the climatology timescale. Following on from the approach taken by Woods [25] for systems where water is stored mainly in the soil, the main objective of this paper is to construct a simple quantitative understanding of the relative importance of some climate factors in controlling the seasonal variation of water storage in snow. Here we build a simple model of the seasonal snowpack evolution and solve it analytically. The analytical solutions provide insight into interactions among the main controlling factors, in the context of the hydrological cycle.

The approach is climatological in nature, and is intended for understanding dominant controls on snowpack dynamics. We deliberately choose to focus first on climates that are cold enough to have a continuous seasonal snowpack; ephemeral snowpacks will be treated as a future extension to the method. The model is not intended for detailed temporal or spatial simulation of snow conditions. It more suited as a screening tool for identifying dominant controlling features, and for interpretation of output from complex simulation models, for initial investigation of broader-scale questions such as the effect of climate change and climate variability on snow and water resources, or the estimation of seasonal snow storage in ungauged catchments.

1.1. Previous work

We discuss four approaches: classification, analytical, empirical and numerical modeling. The analytical approach taken here is intermediate in complexity between existing classification approaches and more detailed numerical models. The need for a synthesis of snowpack climatology has been previously addressed through classification of seasonal snow cover [23], but not with a view to making quantitative predictions of water fluxes and storages. Sturm et al. [23] characterized seasonal snowpacks in six classes, based on vegetation and meteorological conditions: tundra, taiga, alpine, prairie, maritime and ephemeral, and described the attributes of snowpacks in each class. They also developed a climate-based method for predicting class membership. The present work is complementary to that of Sturm et al. [23], in the sense that it provides more information on timing and amount of water storage and flux, but less information about processes of snowpack formation and structure.

Related analytical studies of seasonal snow dynamics include Hantel and Hirtl-Wielke [6], who study the impacts of temperature trends on the number of days per year of snow cover, and Perona et al. [15], who consider the interannual variability of peak snow water equivalent and date of melt out.

Empirical methods exist to directly predict snow climatology, generally on the basis of elevation and temperature data (e.g. Section 4.7 of Tabler [24]), or by spatial interpolation (e.g. [21]). The methods proposed in this paper provide a similar level of predictive detail, but with more insight into the links between climate and snow storage and fluxes.

Many numerical simulation models of snowpack accumulation and melt already exist, including temperature index models (see e.g. the review by Hock [7]) and energy balance models, e.g., Slater et al. [22], Etchevers et al. [4]. These models operate at timescales shorter than climatology, providing a level of temporal and spatial detail which is far beyond the scope of the present paper. They are well adapted to understanding or estimating the specific time course of the snowpack. They can also be numerically integrated over long time periods to provide information on snowpack climatology, but results are difficult to interpret at that timescale.

The approach of the present paper may be able to mimic some climatology-scale features of output from detailed simulation models, using less detailed input and simpler dynamics, to provide understanding of system behavior at seasonal timescales which can be easily compared and interpreted across locations (at the expense of having less predictive power and lower accuracy).

1.2. Outline

This paper develops an analytical seasonal model of snow accumulation and melt, identifying dimensionless variables controlling the system response, with examples from six contrasting locations. From the analytical solutions, we show how the sensitivity of snow water storage to climate variability can be estimated. The paper concludes with an assessment of limitations of the model, possible extensions, links to an existing snow classification, interpretation of the results, and prospects for application of the approach.

2. Model development

2.1. Snow accumulation and melt model

We assume that precipitation, P, falls as snow if temperature T is less than a fixed threshold T_0, and as rain otherwise (more complex schemes are common in practice). We also assume that snow melts according to a melt factor, K (e.g., depth of water per unit time per °C). Then the melt rate at time t is $K(T - T_0)$ (depth of water per unit time), provided that $T > T_0$ and there is still snow left in the snowpack. We will assume here that K is constant, but this assumption could be relaxed provided the seasonal variability in K is known and can be simply described. Sublimation is not modeled because the available predictive models are either specific to particular environments [9,10] or require data that are not generally available [1,16,17]. Using these very simple assumptions, the seasonal snowpack storage at a point, W_s, evolves over time according to this differential equation:

$$\frac{dW_s}{dt} = \begin{cases} P, & \text{if } T \leqslant T_0, \\ -K(T - T_0), & \text{if } T > T_0 \text{ and } W_s > 0, \\ 0, & \text{if } T > T_0 \text{ and } W_s = 0. \end{cases} \quad (1)$$

Eq. (1) is a very simple temperature index model. It is a point-scale model that ignores any spatial variability or vertical structure, and neglects all lateral fluxes (e.g. blowing snow, avalanches). This equation can be solved by specifying W_s at an initial time, along with values of P, T and K at all times. Usually it is solved by numerically integrating the model forward in time. In this paper we solve the equation analytically, for a special case with an idealized climate. However, the goal of the paper is more than just the solution of the equation. We wish to solve it in a way that concisely summarizes and provides insight into interactions among the driving variables: that is why we will seek solutions in terms of dimensionless similarity variables.

2.2. Seasonal climate model

Suppose that, at a point, the typical seasonal variability of precipitation and air temperature can be modeled as sine curves [11,12,19,25], that is

$$P(t) = \overline{P}[1 + \delta_P \sin(2\pi(t - s_P)/\tau)], \quad (2)$$

$$T(t) = \overline{T} + \Delta_T \sin(2\pi(t - s_T)/\tau), \quad (3)$$

where t is time (e.g., measured in units of years, with $t = 0$ arbitrarily chosen at the end of April), s_P is a phase shift [T] of precipitation, and τ is the duration of the seasonal cycle, which is one year (δ_P with s_P is exactly the same climate as $-\delta_P$ with $s_P + \tau/2$). $P(t)$ is precipitation rate [$L\,T^{-1}$] at time t, expressed in depth of water per unit time (e.g. mm d^{-1}) with time-averaged mean value $\overline{P}$, and

dimensionless seasonal amplitude δ_P (between −1 and 1). The temperature, $T(t)$, has a time-averaged mean value $\overline{T}$ (e.g. °C), a seasonal amplitude Δ_T (e.g. °C), and a phase shift s_T [T]. (The choice of units for the variables does not affect the solutions, provided that units are used consistently for length, time and temperature.)

Fig. 1 shows sample time series of precipitation and temperature for a year, generated using this simple model. (For simplicity, in the rest of this paragraph we will assume the temperature time-shift $s_T = 0$.) If Δ_T is positive, this corresponds to having the largest seasonal temperatures at the end of July, which is appropriate for the northern hemisphere, while in the southern hemisphere, Δ_T is negative. Seasonal temperature variation is modeled using a sinusoidal term added to the mean temperature, whereas the seasonal variation of precipitation is modeled with a multiplicative term. This simple climate model ignores the effects of both inter-annual variability and sub-seasonal (i.e., synoptic weather system, diurnal) variability, though this assumption will be relaxed in future work. The model ignores spatial variability, though this can be included later, to an extent, once the nature of the spatial variability is described (e.g., dependence on elevation). We also assume that when temperature is below a threshold, T_0, all precipitation falls as snow, and for temperatures above the same threshold, T_0, all precipitation falls as rain.

2.3. Data

The model developments will be illustrated using six SNOTEL stations, which monitor climate and snow conditions in the western USA: relevant attributes of the sites are listed in Table 1. The stations are operated by the Natural Resources Conservation Service of the United States Department of Agriculture, and their data and descriptions of the measurement network and sensors are available from http://www.wcc.nrcs.usda.gov/snow/. Photographs of the six sites used here indicate that they are in clearings adjacent to, or within, forested environments. The characteristics of the data from the SNOTEL network were summarized by Serreze et al. [20].

To estimate the parameters $\overline{T}, \Delta_T, s_T, \overline{P}, \delta_P$ and s_P in at each of the six sites, days which had data available for daily mean temperature (between −25 and +40 °C), daily precipitation and snow water equivalent were selected from each record. This procedure provided record lengths of 19–25 years, generally with 5–10% missing data (13% at CO). The parameters $\overline{T}, \Delta_T$ and s_T shown in Table 1 were estimated by exhaustive search on s_T, combined with least squares regression for $\overline{T}$ and Δ_T; the same method was used to estimate $\overline{P}, \delta_P$ and s_P.

2.4. Solution of seasonal snow model

We denote the times when seasonal changes occur from rain to snow and back to rain as t_s and t_e, respectively; they are the start and end of the snow accumulation period. To obtain solutions for Eq. (1) it will be convenient to first write Eq. (3) in dimensionless form as

$$\frac{T(t) - T_0}{|\Delta_T|} = \overline{T}^* + \mathrm{sgn}(\Delta_T)\sin(2\pi(t - s_T)/\tau), \tag{4}$$

where $\mathrm{sgn}(\Delta_T) = \Delta_T/|\Delta_T| = \pm 1$, and the dimensionless mean temperature, $\overline{T}^*$, is a convenient ratio of temperature differences:

$$\overline{T}^* = \frac{\overline{T} - T_0}{|\Delta_T|}. \tag{5}$$

The variable $\overline{T}^*$ summarizes information about timing of seasonal temperature variations into a single variable. Locations with the same value of $\overline{T}^*$ are similar, in the sense that they have the same fraction of the year below freezing. Fig. 2 shows time series of modeled temperature for two locations with contrasting values of $\overline{T}^*$. The details of the locations are given in Table 1, along with other locations used later in the paper. They are not intended to be representative of any wider region, and simply illustrate a range of sites to which the theory might be applied. Note that changing the sign of Δ_T has no effect on the value of $\overline{T}^*$, but would shift the timing of the temperature cycle by half a year. Climates with values of $\overline{T}^* > 1$ are above freezing all year round, climates with $\overline{T}^*$ close to 0 are below freezing for about half the year (e.g. the UT site in Fig. 2), while climates with $\overline{T}^* < -1$ are below freezing all year round.

In this purely seasonal model we have assumed that the snow accumulates throughout the period from $t = t_s$ to $t = t_e$, without any melting or sublimation (t_s and t_e will be determined shortly). We also assume that the accumulated snow begins melting when

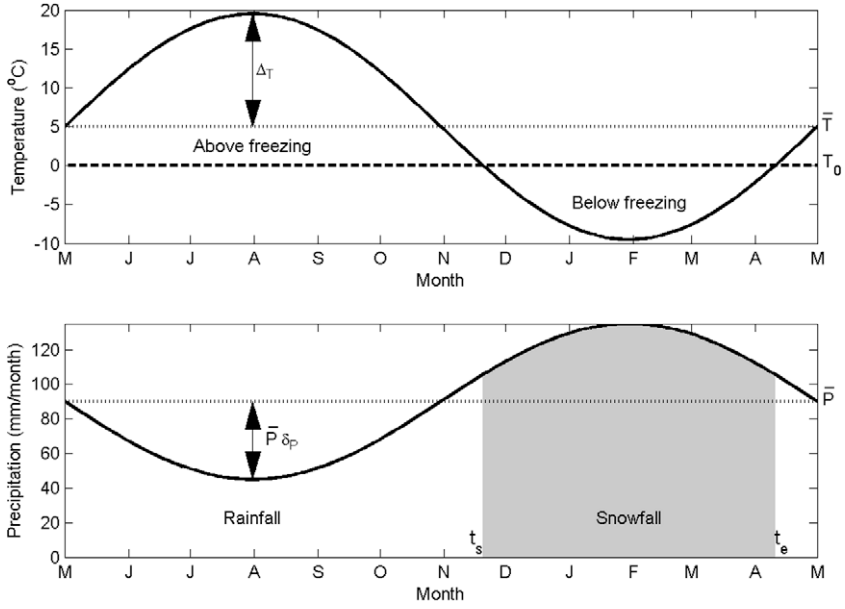

Fig. 1. Simple model of precipitation and temperature, which also shows the start and end of modeled snow accumulation period, as defined by the freezing temperature, T_0. (For simplicity, this example assumes $s_P = 0$ and $s_T = 0$.) The shaded area represents snowfall.

Table 1
Characteristics of SNOTEL measurement sites used as examples, listed from coldest to warmest.

Sym	State	Site name	Climate[a]	Class, Region[b]	Elev. (m)	Lat	Long	$\overline{T}$ (°C)	Δ_T (°C)	S_T (days)	$\overline{P}$ (mm y^{-1})	δ_P	S_P (days)
UT	Utah	Lakefork#1	Dfc	Taiga, 6	3174	40.58	−110.43	−0.8	10.4	−10	651	−0.04	−66
WY	Wyoming	Old Battle	Dsc	Deep Taiga, 7	3048	41.15	−106.97	−0.1	11.6	−9	1244	−0.57	−5
MT	Montana	Flattop Mtn.	Dfc	Maritime, 4	1920	48.80	−113.86	0.7	9.8	−11	1803	−0.48	−13
CO	Colorado	Culebra#2	Dfc	Alpine, 7	3200	37.21	−105.12	1.0	9.4	−12	725	−0.18	98
WA	Washington	Sasse Ridge	Dsb	Maritime, 1	1280	47.38	−121.06	4.6	9.5	−6	1485	−1.03	−26
NM	New Mexico	Silver Crk Divide	Dsb	Maritime, 8	2743	33.37	−108.71	5.3	8.7	−11	858	0.30	63

[a] Köppen–Geiger classifications [14]: Dfc: cold, without dry season, cold summer; Dsb: cold, with dry, warm summer; Dsc: cold, with dry, cold summer.
[b] Class name according to rules of Sturm et al. [23] (note that five of the sites lie close to class boundaries); Region number as defined by Serreze et al. [20].

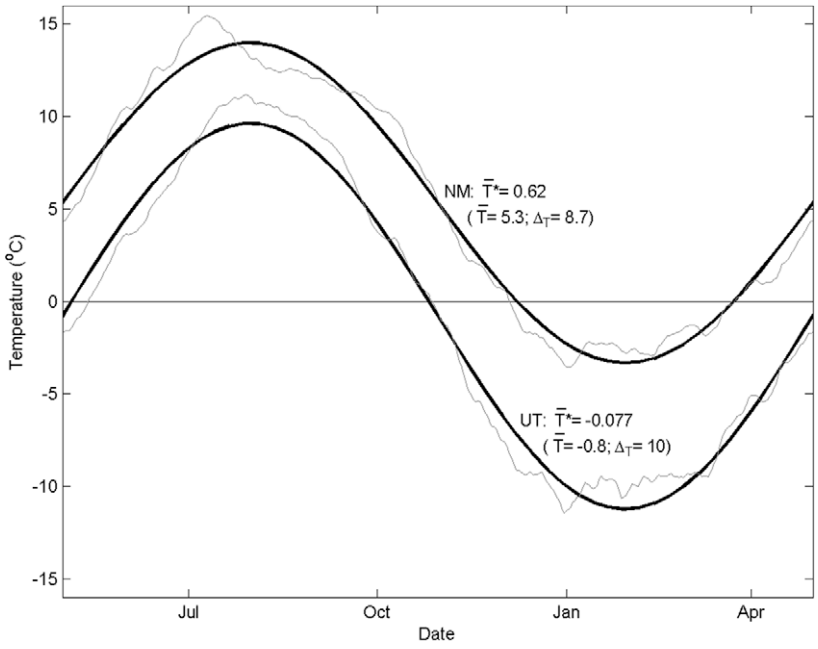

Fig. 2. Modeled seasonal temperature time series at the NM and UT locations (measured climatology for each site is shown in lighter shade for comparison, as 10-day centred moving means). The other sites have similar differences between measured and modeled temperature climatology. Higher values of $\overline{T}^*$ correspond to climates that are above freezing ($T_0 = 0\,^\circ C$) for longer. Note that many combinations of $\overline{T} - T_0$ and Δ_T can result in the same value of $\overline{T}^*$.

seasonal temperature rises above T_0, at time $t = t_e$. Finally, we denote by t_m the time at which the seasonal snowpack is completely melted. The solution for the time variation of snow water equivalent is found by integration of Eq. (1), giving

$$W_s(t) = \begin{cases} W_s(t_s) + \overline{P}\tau\left[\frac{t-t_s}{\tau} - \frac{\delta_P}{2\pi}\left(\cos\left(\frac{2\pi(t-s_P)}{\tau}\right) - \cos\left(\frac{2\pi(t_s-s_P)}{\tau}\right)\right)\right], & t_s < t \leqslant t_e, \\ W_s(t_e) - K|\Delta_T|\tau\left[\overline{T}^*\frac{t-t_e}{\tau} - \frac{\mathrm{sgn}(\Delta_T)}{2\pi}\left(\cos\left(\frac{2\pi(t-s_T)}{\tau}\right) - \cos\left(\frac{2\pi(t_e-s_T)}{\tau}\right)\right)\right], & t_e < t \leqslant t_m, \\ 0, & t_m < t \leqslant t_s + \tau. \end{cases} \quad (6)$$

For a given initial condition, $W_s(t_s)$, the solutions for W_s at t_e and $t_s + \tau$ are of particular interest, since they quantify the maximum and minimum snowpack storage, respectively (given the simple assumptions about seasonality of climate). The first step in linking Eq. (6) to climate characteristics is to find the times t_s and t_e: this is the topic of the next section. Later, we will also determine the peak snowpack storage $W_s(t_e)$, and the time when the snowpack is melted, t_m.

2.5. Snow accumulation period

To determine t_s and t_e we now need to solve Eq. (4) to obtain the times when $T(t) = T_0$, i.e.,

$$\overline{T}^* + \sin(2\pi(t - s_T)/\tau)\mathrm{sgn}(\Delta_T) = 0. \quad (7)$$

This equation has two solutions each year (assuming that $-1 < \overline{T}^* < 1$). The time after $t = s_T$ when $T(t)$ first falls below freezing (T_0) is the start of the snow accumulation period: the relevant solution of Eq. (7) is

$$t_s/\tau = \frac{\sin^{-1}(\overline{T}^*)}{2\pi} + \frac{s_T}{\tau} + \frac{1}{2}I(\Delta_T > 0). \quad (8)$$

$I(\Delta_T > 0)$ is an indicator function which is 1 if $\Delta_T > 0$ and 0 otherwise. The two branches of the above solution correspond to the earth's northern ($\Delta_T > 0$) and southern ($\Delta_T < 0$) hemispheres.

Note that there are special cases where t_s/τ does not have a value in Eq. (8) because $\overline{T}^* > 1$ or $\overline{T}^* < -1$. These cases correspond to climates where the seasonal average temperature is either above or below freezing all year round, and so a modeled snow season cannot be identified. However, if $-1 < \overline{T}^* < 1$, then the modeled

temperature crosses from above freezing to below freezing and back again, during each year.

The start and end of the modeled snow accumulation period are symmetrically located about the coldest time of the year, so $t_e - t_{coldest} = t_{coldest} - t_s$, and so the end of the snow accumulation period is at $t_e = t_{coldest} + (t_{coldest} - t_s) = 2t_{coldest} - t_s$. Since our time origin is at the end of April, the southern hemisphere has $t_{coldest} = \tau/4 + s_T$ (end of July if $s_T = 0$), while the northern hemisphere has $t_{coldest} = 3\tau/4 + s_T$ (end of December if $s_T = 0$). From this we can write

$$t_{coldest}/\tau = \frac{1}{4} + s_T/\tau + \frac{1}{2} I(\Delta_T > 0), \tag{9}$$

$$t_e/\tau = \frac{1}{2} - \frac{\sin^{-1}(\overline{T}^*)}{2\pi} + s_T/\tau + \frac{1}{2} I(\Delta_T > 0). \tag{10}$$

The duration of the snow accumulation period is then found from Eqs. (8) and (10) as

$$\frac{t_e - t_s}{\tau} = \frac{1}{2} - \frac{\sin^{-1}(\overline{T}^*)}{\pi}. \tag{11}$$

Fig. 1 shows t_s and t_e, marked on the modeled times series of temperature. In Fig. 2 we see that the colder Utah (UT) site will have an earlier t_s and later t_e, respectively, than the New Mexico (NM) site. Fig. 3 shows the effect of $\overline{T}^*$ on t_s and t_e: the UT and NM sites are predicted to have the longest and shortest snow accumulation seasons, respectively, of the six example sites.

2.6. Snow accumulation

As noted above, we also use sine curves to model the temporal variation of precipitation. Fig. 4 shows comparisons of measured and modeled seasonal precipitation at the six example sites. This model of seasonal precipitation (Eq. (2)) appears useful for two sites (WY and WA), adequate for two (UT and MT), and poor for two (CO and NM); the bimodal distribution of precipitation in each year is clearly not well modeled at CO and NM. However, the purpose of the model is to estimate seasonal snow climatology, not seasonal precipitation, so we will delay further assessment until the snow predictions have been made.

The proportion of mean annual precipitation which falls as snow, f_s, is found by integrating the modeled precipitation $P(t)$ (Eq. (2)) over the snow accumulation period between $t = t_s$ and $t = t_e$ and dividing by the total annual precipitation ($\overline{P}\tau$):

$$f_s = \frac{t_e - t_s}{\tau} - \frac{\delta_P}{2\pi}[\cos(2\pi(t_e - s_P)/\tau) - \cos(2\pi(t_s - s_P)/\tau)]. \tag{12}$$

Using the results of Appendices A and B to express the difference of cosines as another cosine, and using the previously derived expressions for t_s and t_e, Eq. (12) simplifies to

$$f_s(\overline{T}^*, \delta_P^*) = \frac{1}{2} - \frac{\sin^{-1}(\overline{T}^*)}{\pi} - \frac{\delta_P^*}{\pi}\sqrt{1 - \overline{T}^{*2}}. \tag{13}$$

Note that a new dimensionless variable, δ_P^*, which represents seasonality of precipitation in relation to seasonality of temperature, has arisen as part of the analytical solution, with

$$\delta_P^* = \delta_P \mathrm{sgn}(\Delta_T)\cos(2\pi(s_P - s_T)/\tau). \tag{14}$$

The dimensionless variable δ_P^* concisely summarizes relevant information on the amplitude and phase of both temperature and precipitation into a single variable. From Eq. (13), the mean annual snow fraction, f_s, depends on two dimensionless variables, δ_P^* and $\overline{T}^*$: δ_P^* quantifies the magnitude of the seasonal variation of precipitation, and its temporal distribution relative to temperature; $\overline{T}^*$ is a dimensionless measure of mean temperature. In this context, $\overline{T}^*$ quantifies the amount of time when the temperature is suitable for snow to fall (see Fig. 3 or Eq. (11)), whereas δ_P^* quantifies how much precipitation falls during that part of the year. Fig. 5 shows the effect of dimensionless mean temperature, $\overline{T}^*$, and amplitude of precipitation, δ_P^*, on the fraction of precipitation which falls as snow, f_s.

As expected, warmer temperatures (increasing $\overline{T}^*$) cause a decrease in the fraction of precipitation which falls as snow, so f_s de-

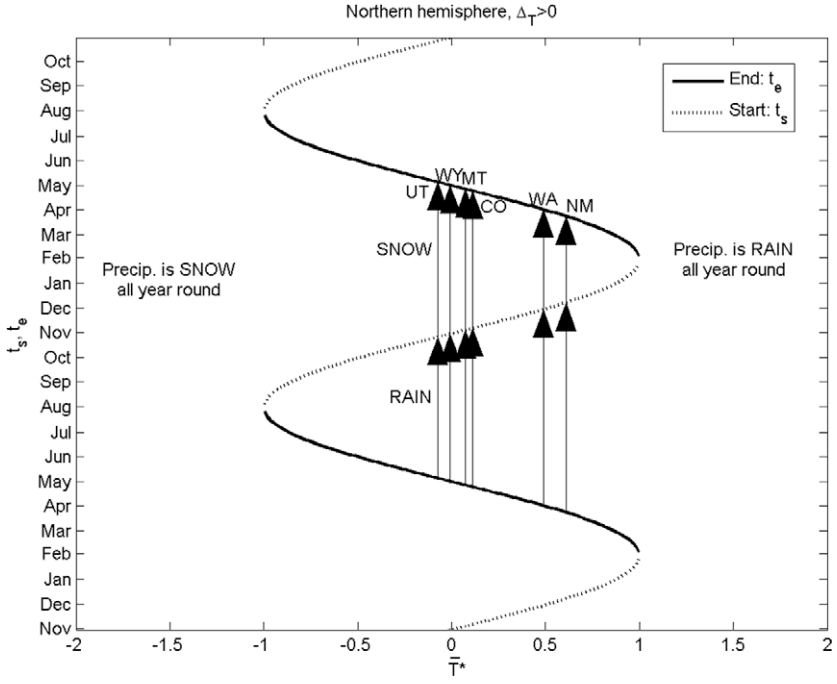

Fig. 3. The estimated effect of $\overline{T}^*$ on the start and end dates for the northern hemisphere snow accumulation period, t_s and t_e, including for six sample locations. For example, at a northern hemisphere location with $\overline{T}^* = 0$ we expect the snow accumulation period to begin near the start of November (i.e., $t_s/\tau = 0.5$) and finish near the start of May (i.e., $t_e/\tau = 1.0$). Results are similar for the southern hemisphere except that all calendar dates are shifted by half a year.

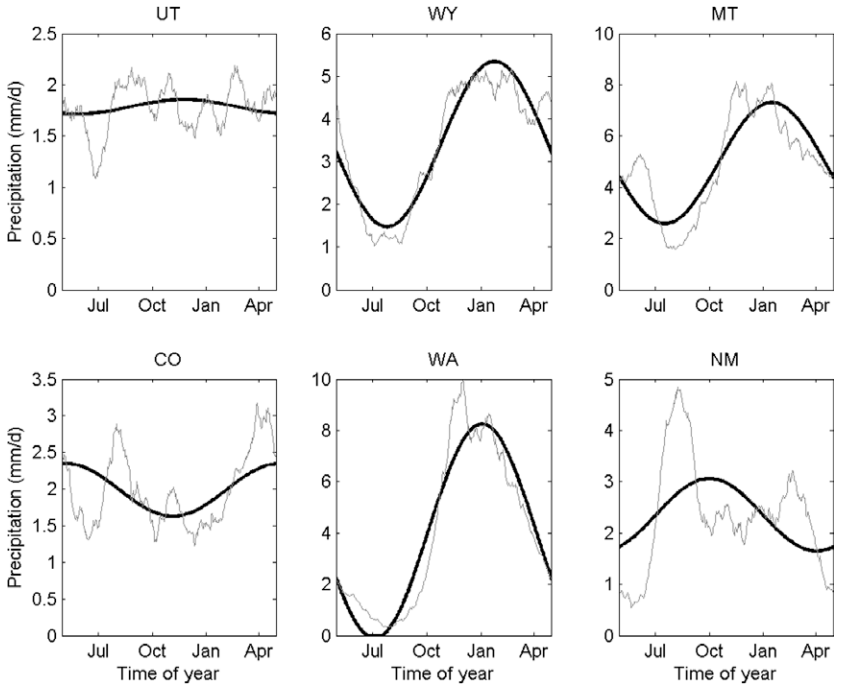

Fig. 4. Modeled (bold) and measured (light) precipitation climatology at the six example sites, labeled by code given in Table 1 (measurements are shown as centred 30-day moving means to emphasise any seasonality).

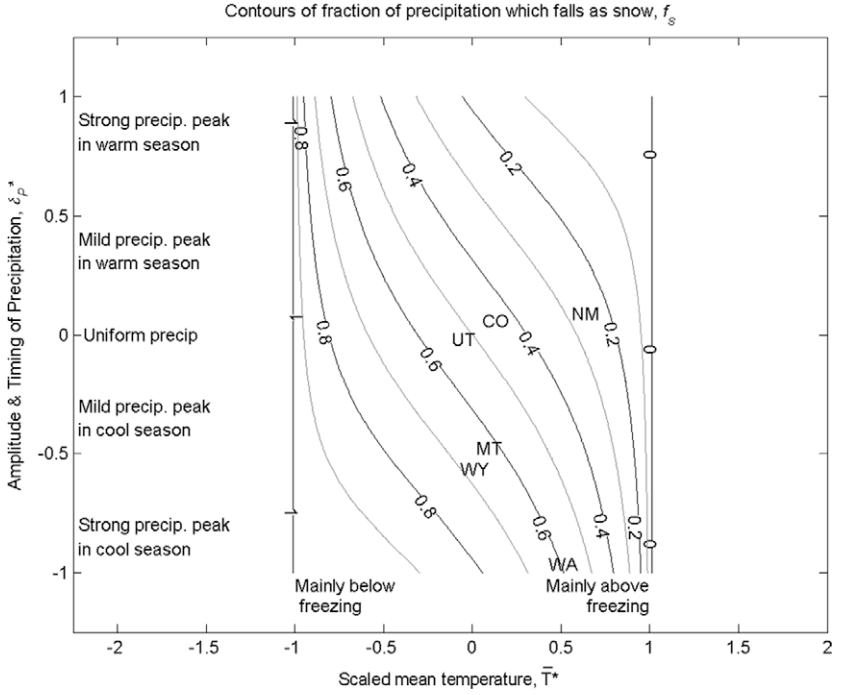

Fig. 5. The effect of dimensionless mean temperature, $\overline{T}^*$, and amplitude of precipitation, δ_P^*, on the fraction of precipitation which falls as snow, f_s. Calculated values of f_s can be read off the plot for six locations.

creases as we move to the right in Fig. 5. As the seasonality of precipitation changes so that relatively more precipitation occurs in the warm season, there is a decrease in the fraction of precipitation that falls as snow (so f_s also decreases as we move upwards in Fig. 5). The WA site has a large snow fraction ($\sim$60%) for what is a relatively warm climate. This happens because most of the precipitation at that site falls in the cold season. In Fig. 6, specific examples of the seasonal patterns of modeled temperature and precipitation are shown for selected values of $\overline{T}^*$ and δ_P^*, to illustrate how these two variables interact to determine the relative proportions of rain and snow. The top row and left column of Fig. 6 illustrate conditions more extreme than any of the six example locations.

Finally, we can substitute the above results for t_s (Eq. (8)), t_e (Eq. (10)), and f_s (Eq. (13)) into the first branch of Eq. (6), to obtain the snowpack storage at t_e.

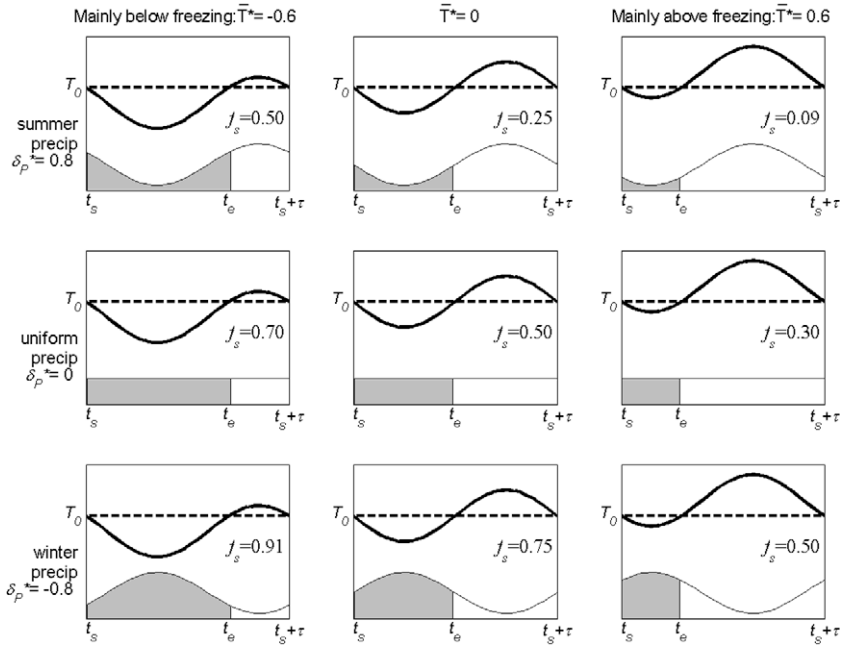

Fig. 6. Examples of the effects of δ_P^* and $\overline{T}^*$ on timing and rate of snowfall (shaded area) and rainfall. Larger snow fractions are predicted for more negative values of δ_P^* and $\overline{T}^*$ (shown at lower left). The heavy solid line represents temperature, and dashed line is freezing temperature. Note that time origin in all plots is at t_s, which may be a different absolute time in each case. (The vertical axis represents both temperature and precipitation rate.)

$$W_s(t_e) = W_s(t_s) + \overline{P}\tau\left[\frac{1}{2} - \frac{\sin^{-1}(\overline{T}^*)}{\pi} - \frac{\delta_P^*}{\pi}\sqrt{1-\overline{T}^{*2}}\right] = W_s(t_s) + \overline{P}\tau f_s(\overline{T}^*, \delta_P^*). \quad (15)$$

2.7. Snow melt

The first question to ask about seasonal snowmelt (within the temperature index framework) is whether there is sufficient warmth available to melt the snowpack. We define the potential melt, $PM(t_1, t_2)$ as the snow water equivalent (e.g., mm of water per unit area) that could be melted between times t_1 and t_2. In this case the time period of interest is from the end of a snow accumulation period $(t = t_e)$ to the beginning of the next snow accumulation period $(t = \tau + t_s)$. If snow is present, the melt rate is $K(T(t) - T_0)$, and $T(t)$ is given by Eq. (3), so

$$PM(t_1, t_2) = K|\Delta_T|\tau\left[\overline{T}^*\frac{t_2 - t_1}{\tau} - \frac{\mathrm{sgn}(\Delta_T)}{2\pi}[\cos(2\pi(t_2 - s_T)/\tau) - \cos(2\pi(t_1 - s_T)/\tau)]\right]. \quad (16)$$

Applying this result to the period when temperature is above zero, between $t_1 = t_e$ and $t_2 = t_s + \tau$,

$$PM(t_e, \tau + t_s) = K|\Delta_T|\tau\left[\overline{T}^*\left(\frac{1}{2} + \frac{\sin^{-1}(\overline{T}^*)}{\pi}\right) + \frac{\sqrt{1-\overline{T}^{*2}}}{\pi}\right] = K|\Delta_T|\tau g(\overline{T}^*). \quad (17)$$

The potential melt from the end of a snow accumulation period to the beginning of the next snow accumulation period, given by Eq. (17), is a function of $K|\Delta_T|\tau$ and $\overline{T}^*$. The term $K|\Delta_T|\tau$ provides a characteristic annual melt depth for a location with $\overline{T}^* = 1$ (minimum seasonal temperature = T_0), and the term $g(\overline{T}^*)$ captures the effect of warm season duration on potential melt (note $g(\overline{T}^* = 1) = 1$, which justifies the characteristic annual melt depth chosen here). Fig. 7 shows this dimensionless potential melt function $g(\overline{T}^*)$ where

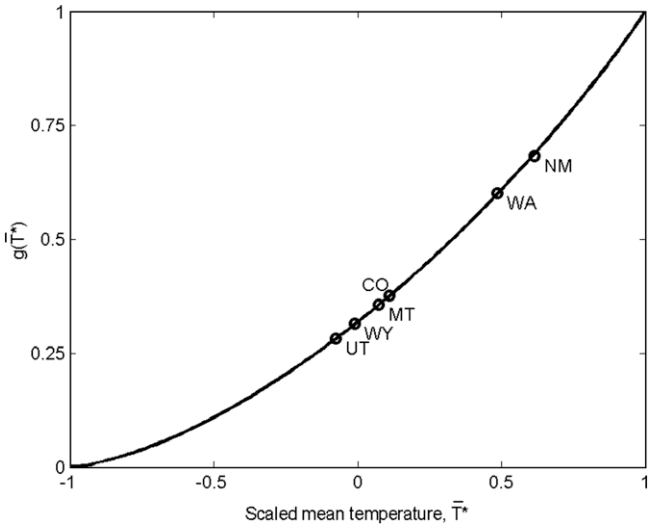

Fig. 7. The function $g(\overline{T}^*)$, with calculated values noted for six locations.

$$g(\overline{T}^*) = \overline{T}^*\left(\frac{1}{2} + \frac{\sin^{-1}(\overline{T}^*)}{\pi}\right) + \frac{\sqrt{1-\overline{T}^{*2}}}{\pi}. \quad (18)$$

For a given seasonal temperature amplitude, $|\Delta_T|$, the function $g(\overline{T}^*)$ measures the effect of dimensionless mean temperature on the potential melt, and is directly proportional to the melting degree–days in an average melt period.

2.8. Comparing snowfall to snowmelt

It will be convenient to define a new dimensionless variable, the dimensionless precipitation rate $\overline{P}^*$, which compares the average precipitation rate, $\overline{P}$, to the characteristic melt rate (for a site with $\overline{T}^* = 1$), $K|\Delta_T|$, giving

$$\overline{P}^* = \frac{\overline{P}}{K|\Delta_T|}. \tag{19}$$

The product $\overline{P}^* f_s(\overline{T}^*, \delta_P^*)$ is a dimensionless measure of the seasonal peak snow accumulation. If $g(\overline{T}^*) < \overline{P}^* f_s(\overline{T}^*, \delta_P^*)$ then there is not enough energy, on average, to melt the snow that falls at this location, according to this simple model. Given these assumptions, such places are a source of snow for glaciers, avalanches, windblown snow or other transport processes. For the situations where there is enough energy to melt the seasonal snowpack, i.e., provided that

$$g(\overline{T}^*) \geqslant \overline{P}^* f_s(\overline{T}^*, \delta_P^*), \tag{20}$$

we need to solve the following equation to get the time, t_m, at which the pack is entirely melted:

$$\overline{P}\tau f_s(\overline{T}^*, \delta_P^*) = PM(t_e, t_m). \tag{21}$$

Eq. (21) equates the amount of snow that accumulates to the melt over the time from the end of the snow accumulation period, t_e, to the (yet to be determined) end of the melt period, t_m. Using Eq. (16) for $PM(t_e, t_m)$, we can expand Eq. (21) and simplify to obtain

$$\overline{P}^* f_s(\overline{T}^*, \delta_P^*) = \overline{T}^* \frac{t_m - t_e}{\tau} - \frac{\mathrm{sgn}(\Delta_T)}{2\pi}\left(\cos\left(\frac{2\pi(t_m - s_T)}{\tau}\right) - \cos\left(\frac{2\pi(t_e - s_T)}{\tau}\right)\right). \tag{22}$$

The only unknown in this equation is t_m/τ, which appears twice. By referring to Eq. (10) for t_e, we can see that Eq. (22) is an implicit equation for t_m/τ as a function of two main dimensionless variables, $\overline{T}^*$ and $\overline{P}^* f_s(\overline{T}^*, \delta_P^*)$, as well as the timing variable, $\mathrm{sgn}(\Delta_T)$, which simply shifts the solution by half a year as required. An analytical solution for t_m/τ is not available, but is straightforward to obtain numerically by any standard root-finding technique, searching on the interval from t_e/τ to $(t_s + \tau)/\tau$ (after first checking that Eq. (20) holds).

It follows directly from the definitions of t_s and t_m that the duration of the modeled snow-free period is $t_s + \tau - t_m$.

Fig. 8 shows how the end of the melt period, t_m/τ, depends on dimensionless mean temperature, $\overline{T}^*$, and on the ratio of snow accumulation to characteristic snowmelt, $\overline{P}^* f_s(\overline{T}^*, \delta_P^*)$. There are no values of t_m/τ in the upper left of the plot because in those cases there is not enough energy to melt the accumulated snow before the next snow accumulation period begins. The line defining this region is $g(\overline{T}^*)$.

The contours of time at end of melt period show the behavior that is expected: as the mean temperature ($\overline{T}^*$) decreases (moving leftward in Fig. 8), the time at end of melt is delayed longer and longer. As the size of the relative snowpack increases (moving upward in Fig. 8), the time at end of melt is also delayed longer and longer. Snowmelt concludes earlier for warmer temperature on smaller snowpacks. The time at which melt ends depends partly on when the snow accumulation period ended (controlled by $\overline{T}^*$) and partly on the time needed to melt the snowpack (controlled by both $\overline{T}^*$ and $\overline{P}^* f_s(\overline{T}^*, \delta_P^*)$).

Fig. 9 shows contours of the duration of the melt period. The results are mainly as would be expected, except for the downward turn of the contour lines on the far right of Fig. 9, which is discussed below. As expected, if the relative snowpack size increases (moving upward in Fig. 9), then the duration of the melt period increases. Similarly, for a given relative snowpack size, as mean temperature ($\overline{T}^*$) increases from $\overline{T}^* = -1$, the melt period gets slightly shorter, which is also as expected.

However, as $\overline{T}^*$ increases through to the largest values of $\overline{T}^*$, the melt period begins to lengthen again. This predicted effect is more pronounced for larger snowpacks. It seems counterintuitive, and could provide an interesting test of the theory. The features of the model that lead to this prediction are: (i) the assumed purely sinusoidal variation of temperature with time, and (ii) the assumption of a clearly-defined change from snowfall to melting as temperature rises above the freezing point. In relatively warm climates (with large $\overline{T}^*$), the start of the melt period occurs at a time when modeled temperature is only rising very slowly at the time it crosses the freezing temperature. Thus in these warm climates the beginning of the melt period has temperatures which

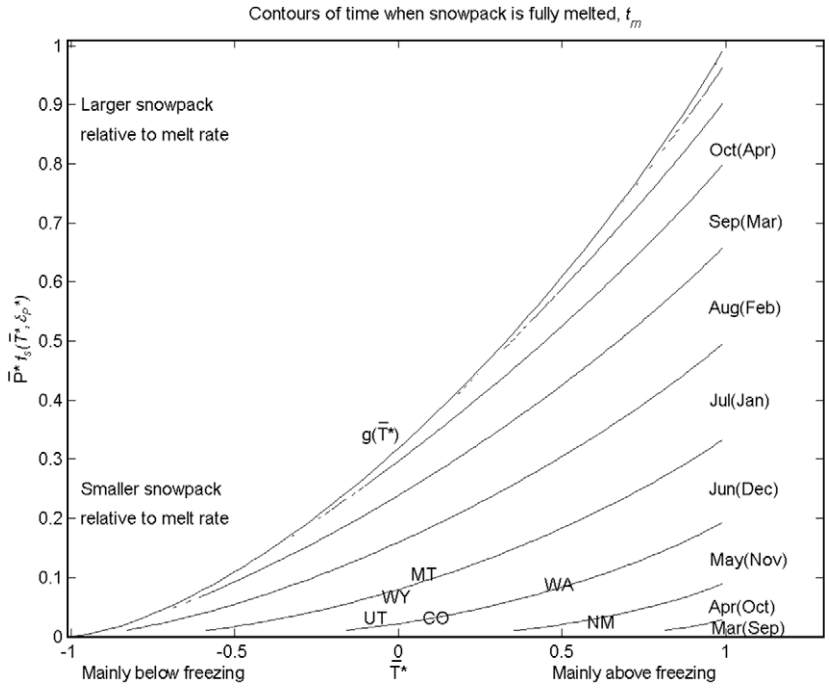

Fig. 8. The effect on the end of the melt period, t_m/τ, of dimensionless mean temperature, $\overline{T}^*$, and of the ratio of snow accumulation to characteristic snowmelt, $\overline{P}^* f_s(\overline{T}^*, \delta_P^*)$. The contour lines are at month boundaries, and month labels indicate times for the northern (southern) hemisphere. Calculated values are shown for six locations.

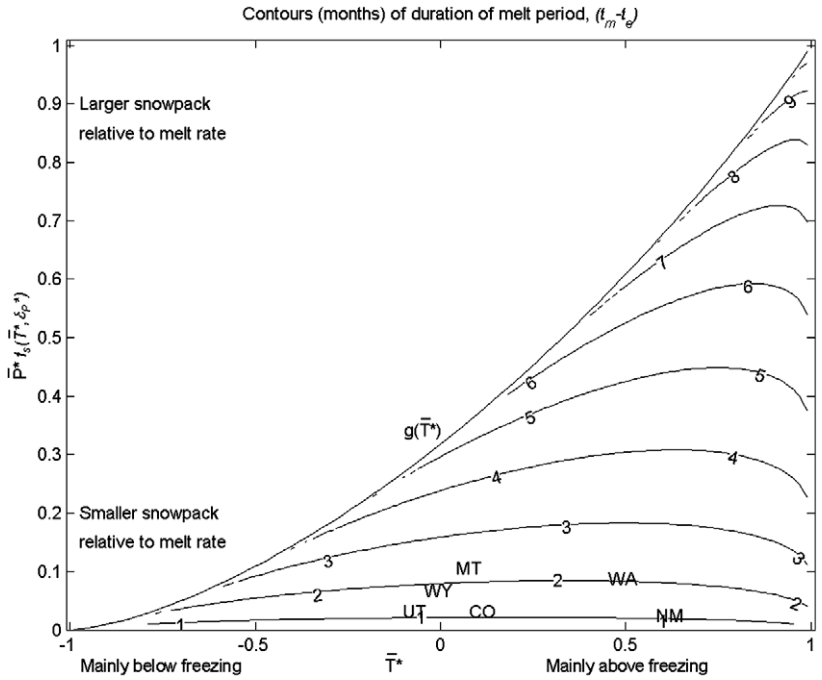

Fig. 9. The effect on the duration of the melt period, $(t_m - t_e)/\tau$, of dimensionless mean temperature, $\overline{T}^*$, and of the ratio of snow accumulation to characteristic snowmelt, $\overline{P}^* f_s(\overline{T}^*, \delta_p^*)$. Contoured values indicate the number of months of snowmelt. Calculated values can be read off the figure for the six example locations.

are only just above freezing for longer than is the case in moderately cool climates (e.g., $\overline{T}^* = 0$), where temperature increases quite steeply as it rises through freezing. It may be that the predicted peak in length of melt period for $\overline{T}^*$ near 1 and large $\overline{P}^* f_s(\overline{T}^*, \delta_p^*)$ in Fig. 9 is simply an artifact of the rather simple assumptions in the model, in which case we would not expect to see the same prediction from a model that uses more detail for its climate inputs. If a real-world example of this phenomena does exist, it will be in a climate which is both warm (short cold season, warmer than the NM example) and wet (very high cold season precipitation – much more than the WA example). Perhaps it could be more readily investigated with data from another planet or another climate epoch.

Fig. 10 shows some specific examples of the snowpack dynamics summarized in Figs. 8 and 9, for selected large, medium and small snowpacks, being melted in four different temperature

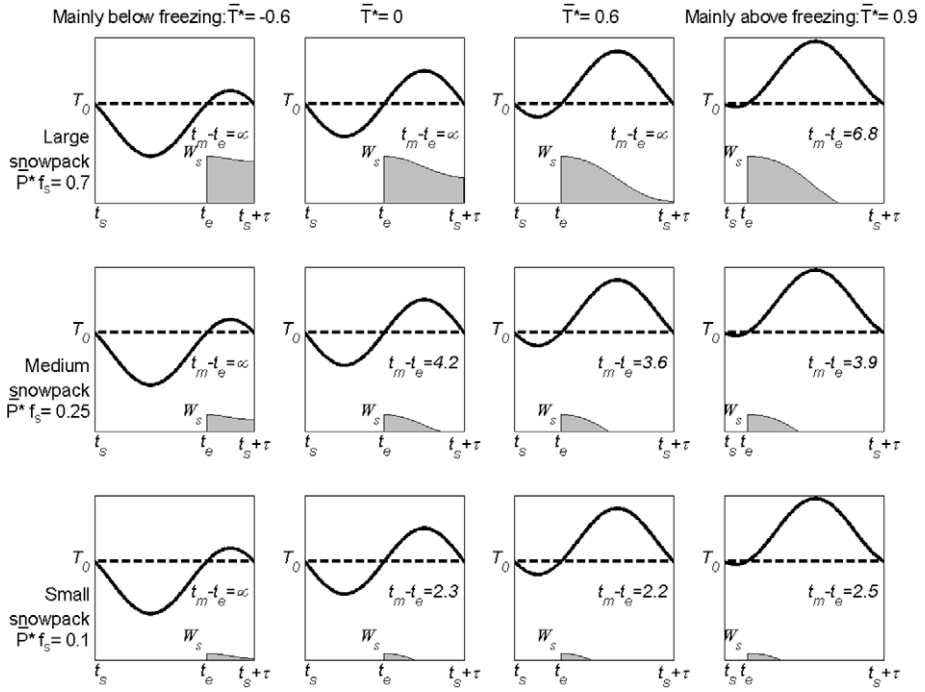

Fig. 10. Examples of the effect of $\overline{T}^*$ and $\overline{P}^* f_s(\overline{T}^*, \delta_p^*)$ on duration of melt period, t_m, (noted in months: $t_m - t_e = \infty$ indicates that the snowpack never melts). Note that these plots use t_s as the time origin; t_s may be a different absolute time in each case. Shaded area shows snowpack, solid line shows temperature, and dashed line is freezing temperature. (Vertical axis indicates temperature and snowpack storage.)

regimes. The time taken to melt the snowpack, $t_m - t_e$, is noted on each plot. The upper two rows of the figure are for much larger snowpacks than at any of the six sample sites. Some of the model snowpacks do not melt during the warm season, and instead represent glacier source areas.

2.9. Dimensionless solution

The solutions above can be written in dimensionless form if we choose a suitable scaling for the snowpack storage. Here we choose $\overline{P}\tau$, the average annual precipitation, as the scaling variable for snowpack storage, and define a dimensionless snowpack storage as

$$W_s^*(t) = \frac{W_s(t)}{\overline{P}\tau}. \tag{23}$$

It then follows that Eq. (6) can be written as

$$W_s^*(t) = \begin{cases} W_s^*(t_s) + \left[\frac{t-t_s}{\tau} - \frac{\delta_P}{2\pi}\left(\cos\left(\frac{2\pi(t-s_P)}{\tau}\right) - \cos\left(\frac{2\pi(t_s-s_P)}{\tau}\right)\right)\right], & t_s < t \leqslant t_e, \\ W_s^*(t_e) - \frac{1}{\overline{P}^*}\left[\overline{T}^*\frac{t-t_e}{\tau} - \frac{\mathrm{sgn}(\Delta_T)}{2\pi}\left(\cos\left(\frac{2\pi(t-s_T)}{\tau}\right) - \cos\left(\frac{2\pi(t_e-s_T)}{\tau}\right)\right)\right], & t_e < t \leqslant t_m, \\ 0, & t_m < t \leqslant t_s + \tau, \end{cases} \tag{24}$$

with t_s, t_e and f_s defined in Eqs. (8), (10) and (13) respectively. From Eq. (24) it follows that dimensionless snowpack storage is a function of dimensionless time, $\overline{T}^*, \delta_P^*$, and $\overline{P}^*$. The largest value of $W_s^*(t)$ each year is predicted to be $f_s(\overline{T}^*, \delta_P^*)$. To fully specify the solution, it is also necessary to provide values for $(\mathrm{sgn}\Delta_T), s_T$ and s_P. Eq. (24) does not apply to cases where there is insufficient energy to melt the seasonal snowpack (e.g. glacier); this condition can be checked by ensuring that $g(\overline{T}^*) \geqslant \overline{P}^* f_s(\overline{T}^*, \delta_P^*)$ (see Eq. (20)).

2.10. Model summary

By assuming a temperature index model of snowpack storage (Eq. (1)), and assuming that temperature and precipitation have only a seasonal variation with time (Eqs. (2) and (3)), we have found expressions for: (i) the predicted time at which snow accumulation begins (Eq. (8)), reaches its peak (Eq. (10)), and finishes melting (Eq. (22)); (ii) the predicted fraction of precipitation that falls as snow (Eq. (13)), and the climatological variation of seasonal snow storage through the year (Eq. (24)). These expressions depend mainly on three dimensionless variables: $\overline{T}^*, \delta_P^*$, and $\overline{P}^*$.

3. Applications of model

Since these expressions depend on a small number of input variables, they can provide insight into how interactions between temperature and precipitation affect snow climatology, and the sensitivity of seasonal snow storage to climate. Here we apply the equations to prediction of SWE at our six example sites, and derive a set of climate sensitivity equations.

3.1. Estimating seasonal snow climatology

3.1.1. Methods

Using only the summary data for climate shown in Table 1 ($\overline{T}, \Delta_T, s_T, \overline{P}, \delta_P, s_P$), along with an assumed melt factor of $K = 3$ mm d^{-1} °C^{-1} (see e.g. the range of values in Hock [7]) and a threshold $T_0 = 0$ °C, it is straightforward to use Eqs. (23) and (24) to estimate the point-scale climatology of snow water equivalent.

To assess the model, daily time series of measured snow water equivalent are available from the SNOTEL network for the six sites listed in Table 1, which sample some of the snow climates present in the western USA. Measured average annual peak SWE ranges from 200 to 400 mm (NM, CO and UT) to more than 1000 mm (WY, MT and WA), and the date of average annual peak SWE ranges from mid-March (NM) to early May (WY). It is important to note that this is not a comprehensive sample of snow climates: these six sites all have continuous snow cover for 3–6 months.

The measured data used here are the climatological mean values of SWE for each day of the year, measured at the monitoring site using a snow pillow (see e.g. [20] for details). The start and end dates for measured and modeled time series were calculated by finding the dates when 10% of the peak SWE had accumulated or only 10% was remaining [5]. This 10% threshold was used to avoid the effects of interannual variability on the SWE climatology, since the longest snow seasons are caused by extreme years, rather than typical years, and so could not reasonably be predicted by this climatological model.

3.1.2. Evaluation

An initial evaluation of the model can be based on Table 2 and Fig. 11, which shows time series of measured and modeled snow water equivalent (SWE). The model reproduces the general magnitude, shape and timing of the observations at these six sites (Fig. 11), albeit with some significant deviations. This result suggests that the very simple climate description contains useful information about snow storage in these places. The estimates of peak SWE are within ±5% of observed values, and estimated accumulation typically starts too late by 1 week, peaks at the right time on average, and melts out 10 days too early. We discuss results for selected sites in more detail below.

Overall the method estimates the peak SWE at these six stations to within ±5%, which is a good result for a simple model, though not surprising given that the total precipitation recorded at the site is an input to the model. Precipitation is measured using an Alter wind shield to maximize catch efficiency, and the data is subject to the quality assurance procedures of the NRCS, but is otherwise uncorrected. To predict the peak SWE correctly at these sites, the model need only represent the seasonal climate patterns adequately and correctly partition the precipitation into rain and snow. The relatively small errors in peak SWE at these six sites indicate that this was achieved in spite of the poor representation of precipitation at some sites. This justifies the use of the sinusoidal curve for precipitation at these sites, in the context of this purely seasonal model. However, it may be that the goodness of fit is partly due to compensating errors in the model (for example, the poor fit to seasonal precipitation at NM may be compensated for by unaccounted diurnal fluctuations in temperature, which may also have an effect on snowpack timing).

These six examples include two sites where we expected difficulties for this modeling approach. The seasonal pattern of precipitation for the sites in New Mexico (NM) and Colorado (CO) are bimodal (Fig. 4), so that the assumed sinusoidal model is a poor fit. Poorer predictions of snow water equivalent (SWE) might be expected for these two sites, relative to the other four. This expectation is not well supported by the summary of results in Table 2: while the NM site has a large error for melt date (the model is 20 days early), the MT site has a similar error for melt date. The CO site is quite well modeled, for reasons which are unclear. The larg-

Table 2
Summary of prediction errors for six example sites. Each error is calculated as predicted value minus observed value. Fig. 11 shows more details of predictions. The last 3 columns give values of dimensionless variables used to make predictions.

Site	Peak SWE error (%)	Start date error (d)	Peak date error (d)	End date error (d)	Accumulation duration error (d)	Melt duration error (d)	$\overline{T}^*$	δ_P^*	$\overline{P}^*$
UT	5.0	5	22	−8	17	−30	−0.08	−0.02	0.03
WY	1.5	7	−11	−8	−18	3	−0.01	−0.57	0.07
MT	2.1	4	0	−18	−4	−18	0.07	−0.48	0.11
CO	1.2	3	6	−3	3	−9	0.11	0.06	0.03
WA	3.7	15	−9	−11	−24	−2	0.49	−0.97	0.09
NM	−1.2	9	−5	−20	−14	−15	0.61	0.09	0.02
Mean abs error	2.4	7.3	8.8	11.3	13.5	12.8			
Mean error	2.0	7.3	0.5	−11.3	−6.8	−11.8			

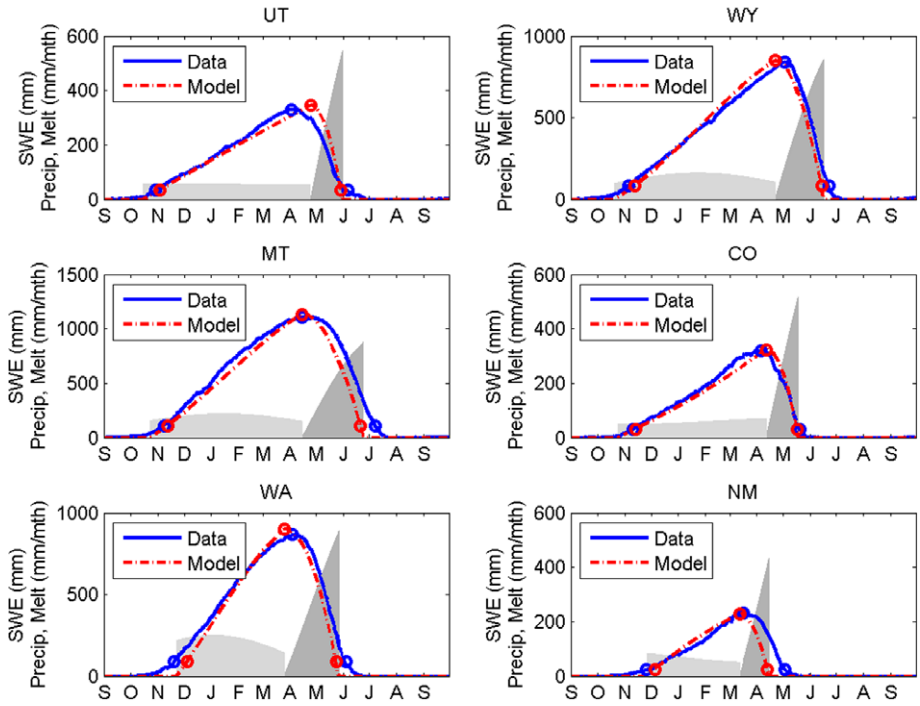

Fig. 11. Comparison of measured (solid lines) and modeled (broken lines) time series of average snowpack storage for each day of the year, at six locations. Circles on measured and modeled traces indicate the peak SWE and the dates near the start and end of the snow season when storage = 10% of peak SWE. These dates are used in constructing Table 2. Light shaded area at left indicates modeled snowfall rate, and darker area at right indicates melt rate. Total melt equals total snowfall.

est errors are with the UT site which peaks three weeks late, and then melts a week too early.

The timing predictions do show some reasonably consistent limitations: the modeled start dates for snow accumulation are too late by 5–15 days, while the other modeled melt date predictions are too early by 3–20 days. While peak timing predictions are unbiased, they do display significant scatter about the measured values. These prediction errors could be caused by model structure errors (e.g. missing or inaccurate process representations), parameter errors, or model forcing errors. The choice of T_0 affects the dates for the start and peak of snow accumulation: typical literature values range from 0 to +2 °C (e.g. [26]). The choice of melt factor K has a significant influence on melt out dates and is subject to considerable uncertainty. The value $K = 3$ mm d^{-1} °C^{-1} was a somewhat arbitrary choice within the range of published values; the bias in estimated time of melt at these six sites can be altered significantly by using $K = 2$, or $K = 4$, both of which are also in the range of literature values. Similarly, one could focus the estimation of the temperature parameters $\overline{T}, \Delta_T, s_T$ on the times of year when temperature is close to freezing (rather than using the whole year), and the estimation of $\overline{P}, \delta_P, s_P$ to times of year when temperature is below freezing. This could increase model precision, but at the expense of turning a simple method into a more complex one. Detailed investigations into parameter estimation are not relevant at this early stage of model development. The purpose of the model is more insight, rather than more accurate prediction.

Fig. 11 also includes modeled time series of snowfall rate, which varies in time according to the fitted sine curve for precipitation (and is nonzero only between t_s and t_e), and the melt rate, which is proportional to temperature – T_0 and is nonzero only when temperature is above T_0 and snow is still present. The figure clearly illustrates that (point-scale) melt is a rapid hydrological process.

3.1.3. Uncertainty in parameters and climate forcing

We can make estimates of the uncertainties in model output that might be expected due to uncertainties in estimating model parameters T_0 and K. This is possible because of the simplifying assumptions we have made to minimise the number of input

parameters, and the use of dimensionless parameters, which make it possible to compare apparently disparate factors.

For the parameters T_0 and K, we first consider the impacts on snow accumulation, and then on snow melt. An increase of one degree Celsius in T_0 (e.g. from 0 °C to 1 °C) would cause a decrease in $\overline{T}^*$ of $1/|\Delta_T|$ (Eq. (5)), i.e. a decrease in $\overline{T}^*$ by about 0.1 (for the sites used here which have $\Delta_T \approx 10$ °C). The times for start and end of snow accumulation would become earlier and later respectively, by 5–10 days each (Eqs. (8) and (10)). That decrease in $\overline{T}^*$ would also cause an increase in f_s of about 0.05 (Fig. 5), and thus an increase in modeled peak SWE of about 5%. An increase of 1 °C in T_0 would affect the duration of melt mainly by the change in f_s, since the contours of melt duration are almost horizontal in the neighborhood of the sites used (Fig. 9). The increase of 0.05 in f_s due to the increased T_0 would cause a 5% increase in $\overline{P}^* f_s$, which Fig. 9 indicates would increase melt duration by 0.5–0.75 months (2–3 weeks).

A change in K would have no effect on accumulation in this simple seasonal model, but it would affect snowmelt. Reducing K to 5/6 of its current value (e.g. from 3 mm d^{-1} °C^{-1} to 2.5 mm d^{-1} °C^{-1}) would increase $\overline{P}^*$ by a factor 6/5 (Eq. (19)), and this would cause $\overline{P}^* f_s$ to also increase by a factor 6/5, i.e. from 0.05–0.1 up to 0.06–0.12. For the sites used here, this would lead to small increases in melt duration, up to 1 week longer.

We can also use these same arguments to examine the role of uncertainty in model input: the effect on the model of temperature bias is the same as the effect of changing T_0. A one degree decrease in mean temperature has exactly the same effect on the model as a one degree increase in T_0 (Eq. (5)), i.e. 5–10 days on start and peak timing, 5% on peak SWE, and 2–3 weeks on melt timing. Increasing precipitation would affect both peak SWE and the time of melt. Increasing precipitation by 20% (i.e. multiplying by a factor 6/5), would not affect f_s but would increase peak SWE by 20% (Eq. (15)). This means an increase in $\overline{P}^*$ by 20% (Eq. (19)), and we have already seen (when considering uncertainty in K) that this magnitude of change in $\overline{P}^*$ causes very small increases in modeled melt duration.

3.1.4. Assessment of model uncertainty

The differences between modeled and measured SWE statistics (except for the peak timing error at UT) are of similar magnitude to the errors estimated above due to uncertainties in model parameters and input. This does not eliminate the possibility that the model structure is incomplete, as we have only conducted very limited testing to date. Overall, the initial results are encouraging, but firm conclusions cannot be drawn from such a small sample, which, for example, has no sites that would be classed by Sturm et al. [23] as very high temperature (ephemeral).

3.2. Sensitivity to long-term climate variation

The analytical model above permits an assessment of the sensitivity of snow to long-term variability in precipitation and temperature. Here we derive the sensitivity equations, and illustrate them graphically. This provides a mathematical expression of the graphical uncertainty analysis of the previous section.

3.2.1. Timing

The model equations for start, end, and duration of snow accumulation (Eqs. (8), (10) and (11), respectively) are affected only by $\overline{T}^*$:

$$\frac{dt_s/\tau}{d\overline{T}^*} = \frac{1}{2\pi\sqrt{1-\overline{T}^{*2}}},$$
$$\frac{dt_e/\tau}{d\overline{T}^*} = -\frac{dt_s/\tau}{d\overline{T}^*} = \frac{-1}{2\pi\sqrt{1-\overline{T}^{*2}}},$$
$$\frac{d(t_e - t_s)/\tau}{d\overline{T}^*} = -2\frac{dt_s/\tau}{d\overline{T}^*} = \frac{-1}{\pi\sqrt{1-\overline{T}^{*2}}}.$$

As expected, the predicted effect (Fig. 12) of an increase in temperature is that the start time of accumulation increases ($d(t_s/\tau)/d\overline{T}^*$ is positive meaning snowpack onset is delayed by a temperature rise), the end time decreases (end of accumulation occurs earlier), and the duration of accumulation decreases.

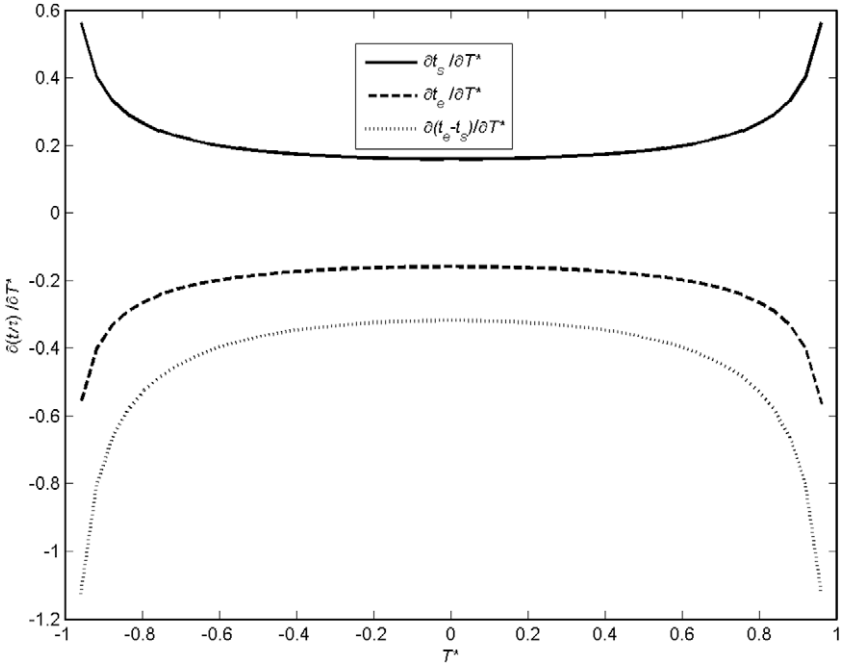

Fig. 12. Sensitivity of snow accumulation timing to dimensionless mean temperature, $\overline{T}^*$.

The graphs of these three sensitivity measures in Fig. 12 shows that the effect of a small change in $\overline{T}^*$ is greatest for values of $\overline{T}^*$ near ±1, and that snow accumulation timing is affected to some extent by a change in $\overline{T}^*$ for all values of $\overline{T}^*$ between −1 and +1.

3.2.2. Snow fraction

The fraction of precipitation which falls as snow (Eq. (13)), f_s, is affected by $\overline{T}^*$ and δ_P^*:

$$\frac{\partial f_s}{\partial \overline{T}^*} = \frac{\overline{T}^*\delta_P^* - 1}{\pi\sqrt{1-\overline{T}^{*2}}},$$
$$\frac{\partial f_s}{\partial \delta_P^*} = \frac{-\mathrm{sgn}(\Delta_T)}{\pi}\sqrt{1-\overline{T}^{*2}}.$$

According to these equations, increases in either $\overline{T}^*$ (warmer climate) or δ_P^* (a change to relatively more warm season precipitation) would lead to reductions in the snow fraction. Whether this would lead to an absolute reduction in snow depth would depend on how total precipitation changed.

From Fig. 13, we can see that the sensitivity of snow fraction to $\overline{T}^*$ depends on the values of both $\overline{T}^*$ and δ_P^*, whereas the sensitivity of snow fraction to δ_P^* depends only on the values of $\overline{T}^*$. Sensitivity to change in $\overline{T}^*$ is most pronounced for values of $\overline{T}^*$ near ±1, although the value of δ_P^* does also affect the sensitivity. In contrast, the effect on snow fraction of a change in δ_P^* is most pronounced near $\overline{T}^* = 0$.

We can interpret Fig. 13 as follows. If the dimensionless mean temperature increases, then the reduction in snow fraction is predicted be greatest for (i) cold locations ($\overline{T}^*$ near −1) with a warm season precipitation peak (ii) warm locations ($\overline{T}^*$ near 1) with a cold season precipitation peak (iii) very cold or very warm locations ($\overline{T}^*$ near −1 or 1) with uniform precipitation through the year. If the seasonality of precipitation changes, then the change in snow fraction will be greatest for locations which are neither especially cold nor especially warm ($\overline{T}^*$ near zero).

3.2.3. Potential melt

The potential melt over the period from t_e to $t_s + \tau$ is dependent on the climate variables $\overline{T}^*$ and $|\Delta_T|$ (see Eqs. (17) and (18)). The sensitivities are:

$$\frac{\partial PM(t_e, t_s+\tau)}{\partial \overline{T}^*} = K|\Delta_T|\tau\left(\frac{1}{2} + \frac{\sin^{-1}(\overline{T}^*)}{\pi}\right),$$
$$\frac{\partial PM(t_e, t_s+\tau)}{\partial |\Delta_T|} = K\tau\left(\frac{1}{2} + \frac{\sin^{-1}(\overline{T}^*)}{\pi}\right).$$

The sensitivity of potential melt to temperature is greatest for values of $\overline{T}^*$ near +1.

3.2.4. Application of climate sensitivity equations

To use the above expressions for climate sensitivity, we can calculate the values of $\overline{T}^*$ and δ_P^* for the "current" climate, and then read the sensitivity values off the figures (or the associated equations). Alternatively, values of $\overline{T}^*$ and δ_P^* for the "current" and "changed" climate can be calculated separately if a specific scenario is available, and values of $t_s, t_e, f_s, PM(t_e, t_s+\tau)$, and t_m calculated for each case, and the results compared directly.

It is important to note that these sensitivity equations depend on the assumptions outlined in the previous section, of which perhaps the most important is the use of the temperature index model with a fixed melt factor, K. It is well known that K is not a physical constant, but a parameter which generally requires calibration, since it collapses many details of the energy balance into a single value, and thus cannot represent complex changes in processes. The uncertainty in estimated dates for snowpack melt (Table 2) are similar in size to the observed advances in melt date over a 40 year period [2], and so at this stage any predicted changes could only be interpreted in a relative sense (change in melt date for a given change in temperature). The purpose of these sensitivity equations is thus to assist in providing insight into the relative importance of changes in temperature and precipitation, rather than in making detailed predictions, for which a more detailed treatment of the processes would be needed.

4. Discussion

4.1. Assumptions and limitations

The theory developed above is dependent on several simplifying assumptions, and many physical details of the real

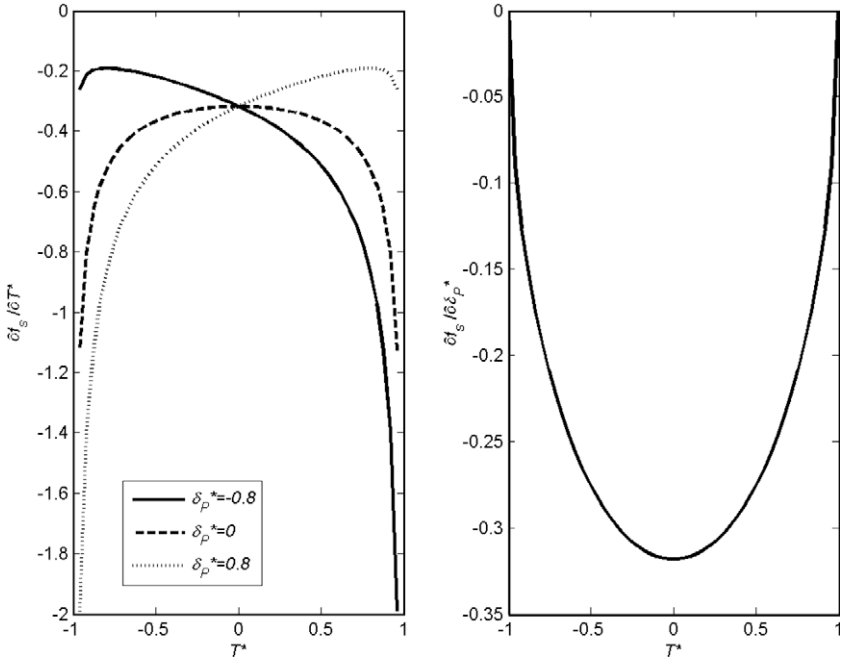

Fig. 13. Sensitivity of snow fraction, f_s, to changes in $\overline{T}^*$ (left, for three values of δ_P^*) and to changes in δ_P^* (right).

environmental system have deliberately been neglected, to seek broad-scale insight into the controlling variables. Some of the limitations of this model when applying it to practical questions are discussed below. All of them should be considered when assessing the validity of this model.

4.1.1. Sublimation

The model excludes sublimation, which is thought to be a significant element of the water balance in some snow-dominated environments (e.g., prairies, forests), but is not well quantified at present [8,10]. If a characteristic sublimation fraction, S, can be estimated (e.g., from leaf area index), then we might decrease the precipitation rate, replacing $\overline{P}$ by $\overline{P}(1-S)$.

4.1.2. Temperature index model

Our use of concepts from the temperature index models requires that the K value be determined when applying the model, but there is only a limited physical basis for K [13], and thus making *a priori* estimates is challenging. The temperature index approach could cause bias in site-specific predictions because K estimates are likely to be quite uncertain. This is a serious problem for a theoretical method, but one that is frequently solved by pragmatic approaches such as regionalization of K values from the literature, hydrological model calibration studies, or very small-scale experimental studies of snow melt. Using energy balance considerations in the snowmelt equations here introduces excessive complexity. It may be possible to improve the physical basis of the model by replacing the temperature model by a radiation model, though this has not yet been explored.

When using the degree–day approach in practice, the K value is understood to change consistently within each year. The assumption made in this paper that the degree–day factor K is constant is not a fundamental limitation – if the seasonal pattern of K can be parameterized, then the equations given here can be generalized.

4.1.3. Non-seasonal climate variability

Although precipitation varies on many temporal scales, the equations here only use seasonal information, and are most suited to continuous seasonal snowpacks. Precipitation as snowfall occurs as distinct events with timescales of the order one day: the seasonal accumulation of such events has recently been considered by Perona et al. [15] leading to an expression for the probability distribution of snow accumulation, but without examining the role of temperature in defining the snow accumulation season. For the objectives of the present paper, a seasonal approach has been adequate for the small sample of study sites here. However, to get insight into controls on variability of snow water equivalent in ephemeral snow locations, non-seasonal fluctuations in both precipitation and temperature will no doubt play an important role. In particular, temperature fluctuations (e.g. diurnal, interannual) play an important role in the non-linear snowpack dynamics for certain climates. We have assumed here that the average inputs can be used to predict the average response – in climates with very strong non-seasonal fluctuations, we would expect the model to fail. An investigation of the impacts of diurnal, synoptic and interannual variations in temperature on snow storage is in progress, along with relevant extensions of the theory presented here.

4.1.4. Topographic effects on snow

Here, we have neglected spatially variable processes which play a key role in understanding how snow dynamics vary with spatial scale – an issue which has great importance for representing snow processes in simulation models (e.g. [3]). Specifically, we cannot yet address the topographically-driven effects of aspect, shading, and redistribution by wind or avalanching on snowpack dynamics. Current understanding of these processes does not readily lend itself to the analytical approach. Related to this, we provide no information on the effect of spatial scale and spatial heterogeneity, and thus no pathway for transferring this information to the catchment scale. These remain active research questions, being addressed by a variety of approaches (and indeed the analytical approach may not necessarily be the most appropriate).

The effect of elevation on climate is a larger-scale source of spatial variability in snow which is more amenable to analytical investigation. In the framework developed above, if L is the lapse rate of temperature with elevation (and one assumes that seasonal amplitude does not vary with elevation), then each unit of elevation rise causes the dimensionless mean temperature, $\overline{T}^*$, to decrease by $L/|\Delta_T|$. Similarly, if precipitation changes systematically with elevation, then the effect of a unit rise in elevation is that $\overline{P}^*$ increases by $N/K|\Delta_T|$, where N is the rate of change of precipitation with elevation. Thus the elevation effect is collapsed into effects on scaled temperature and scaled precipitation, and the equations above can be applied. This provides a simple way to summarize some of the most basic large-scale impacts of elevation on snow dynamics.

4.2. Correspondence to the snow classification of Sturm et al.

Sturm et al. [23] developed a method for using climate and land cover information (temperature, precipitation, vegetation height) to predict snow class (tundra, taiga, alpine, prairie, maritime and ephemeral). Threshold values of 125 and 30 cooling degree months (with $T_c = 10\,^\circ\mathrm{C}$ base temperature) were selected by Sturm et al. [23] to distinguish their low, high and very high temperature regimes. A winter precipitation rate threshold of $P_c = 2\ \mathrm{mm\ d^{-1}}$ was selected for separating low and high precipitation, where winter precipitation was defined as occurring in months with mean temperature less than $T_c = 10\,^\circ\mathrm{C}$. Here we translate those climate thresholds into the context of this paper.

Sturm et al.'s cooling degree month thresholds of 125 and 30 correspond to $\overline{T}^*$ values very close to 0 and 1 respectively, for a reasonable range of temperature regimes and threshold temperature (i.e., $8\,^\circ\mathrm{C} < |\Delta_T| < 20\,^\circ\mathrm{C}$, $-2 < T_0 < 2$). This can be shown by adapting Eq. (16) for use in the cold part of the year and using $T_0 = T_c$ to compute t_s and t_e. If Sturm et al.'s T_c had not been 10 °C then the corresponding values of $\overline{T}^*$ would be different.

Sturm et al.'s winter precipitation rate threshold of $P_c = 2\ \mathrm{mm\,d^{-1}}$ corresponds approximately to $\overline{P}^* f_s = (1 - .9\overline{T}^*)/(K|\Delta_T|)$. This can be shown using Eqs. (11) and (13) with $T_0 = 10\,^\circ\mathrm{C}$ to get the total winter precipitation and the duration of the winter period. The impact of δ_P^* on this result is relatively small, and has been neglected here.

This provides enough information to allow an approximate mapping of the Sturm et al. classes onto the present modeling framework. The information is summarized in Fig. 14 (expanding the lowest part of Fig. 9), on which the $\overline{T}^*$ thresholds are vertical lines, and the $\overline{P}^* f_s$ threshold is a sloping line. Reasonable ranges for K and $|\Delta_T|$ are 1–5 $\mathrm{mm\,d^{-1}\,^\circ C^{-1}}$ and 8–20 °C, respectively. The six example sites are shown on Fig. 14, and their classes can be read from the figure. As noted in Table 1, five of the sites lie close to class boundaries.

An unresolved question which then arises from this proposed correspondence is why Alpine seasonal snow (in the lower right of Fig. 14) is not adjacent to glacier source areas (on the left of the $g(\overline{T}^*)$ line of Fig. 14), given that glacier source areas are typically adjacent to alpine seasonal snowfields in both physical and environmental space.

The modeling framework presented here is not broad enough to include discrimination of low wind and high wind climates. As a result, more than one snow class may correspond to each combina-

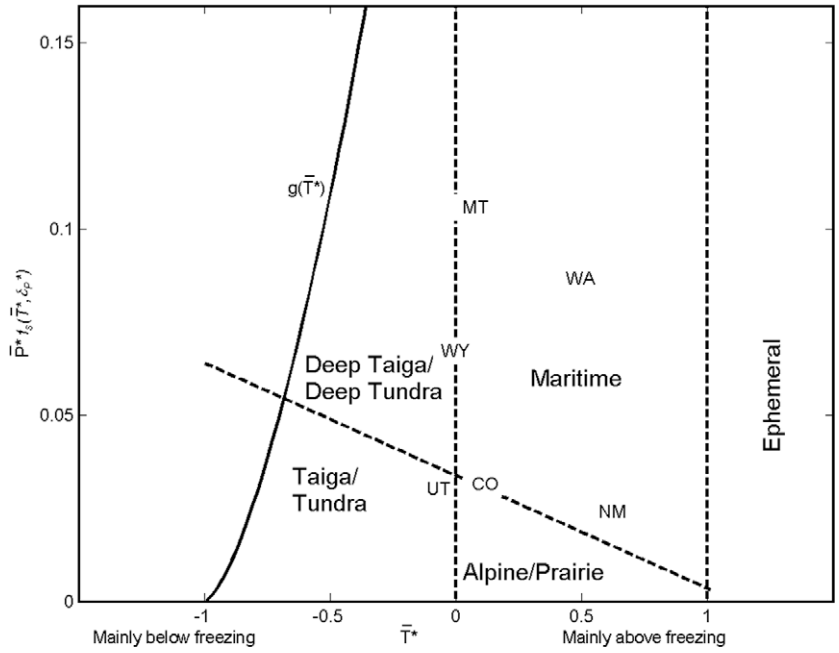

Fig. 14. Mapping Sturm et al. [23] classes onto dimensionless axes (expanding the lowest part of Fig. 9), with six example sites shown. The solid line marked $g(\overline{T}^*)$ indicates the glacier regime boundary of this model. The dashed vertical and sloping lines separate Sturm et al. classes. Note that the precise position of the sloping line can vary, depending on other variables (here $K = 3$ mm d^{-1} °C^{-1} and $|\Delta_T| = 10$ °C).

tion of dimensionless numbers $\overline{T}^*$ and $\overline{P}^*$. The final discrimination of taiga vs. tundra or alpine vs. prairie may be resolved using land surface attributes (especially tall vs. short vegetation), following Sturm et al. [23].

4.3. Use of dimensionless variables for similarity

The solution above identified three dimensionless variables: $\overline{T}^*$ to quantify the temperature regime, δ_P^* to quantify the seasonality of both temperature and precipitation, and $\overline{P}^*$ to quantify the mean precipitation rate relative to a characteristic melt rate. A classical application of dimensionless controlling variables is to identify situations which are similar. In this case we might say that two locations are predicted to be similar in respect of the four seasonal snowpack response variables described above if they have an identical triplet of values for $\overline{T}^*, \delta_P^*$ and $\overline{P}^*$. To determine how close two $(\overline{T}^*, \delta_P^*, \overline{P}^*)$ triplets need to be for "effective" similarity, one can look for example at the spacing of the contours of response variables shown in Figs. 5 and 9. While it is trivial to claim that another place with the same $(\overline{T}^*, \delta_P^*)$ pair as WA will have the same modeled snow fraction as WA, one can also see from Fig. 5 that other combinations $(\overline{T}^*, \delta_P^*)$ could also produce similar snow fractions (e.g. the point labeled MT). From Fig. 9 we can see from the separation of the contour lines that to find two places whose melt period durations are within a month of one another, we typically would need the $\overline{P}^* f_s(\overline{T}^*, \delta_P^*)$ values of the two locations to be within 0.05 of one another. If their $\overline{P}^* f_s(\overline{T}^*, \delta_P^*)$ values differ by more than this, they are not expected to be similar in respect of melt duration.

5. Summary and conclusions

Using an analytical approach, we investigated climate controls on the climatological mean seasonal snowpack. We derived model equations for the peak snow accumulation (as a proportion of annual precipitation), and the start, peak and end of the snow season. Based on our assumptions, three main dimensionless variables have been identified as controlling these responses: $\overline{T}^*$ to quantify the temperature regime, δ_P^* to quantify the seasonality of both temperature and precipitation, and $\overline{P}^*$ to quantify the mean precipitation rate relative to a characteristic melt rate. In this purely seasonal analysis, $\overline{T}^*$ alone determines the start and peak of snow storage (Eqs. (8) and (10)), $\overline{T}^*$ and δ_P^* together determine the peak dimensionless snowmelt storage (relative to annual precipitation, Eq. (13)), and $\overline{T}^*, \delta_P^*$ and $\overline{P}^*$ together determine the time at which the snowpack is completely melted (Eq. (22)). The major interactions of the seasonal temperature with other climate elements are then summarized in Figs. 5 and 9, which provide understanding of seasonal climate controls on snow fraction and snowmelt timing for locations with a continuous seasonal snowpack.

At this point we do not claim that the model derived here is generally accurate or useful, but we note that at six instrumented sites with adequate model inputs, the simple model predicted peak snow water equivalent to within ±5%, with typical timing errors of ±1–2 weeks, without any calibration. The errors are consistent with uncertainties in input and model parameters, but may also be due to model structural errors (e.g., neglect of non-seasonal timescales, use of temperature index model). The analytical form of the model provides insights into the interactions between mean temperature, seasonality of temperature, mean precipitation, seasonality of precipitation, and melt factor for locations with a continuous seasonal snowpack. It can also be linked to the Sturm et al. [23] snow classification system.

If further testing now in progress demonstrates that the model gives adequate estimates of seasonal snowpack response for a wider range of locations, we might envisage applications of this approach to (i) definition of hydrological similarity indices in snow-dominated regions (ii) interpretation of output from complex simulation models covering a wide range of environments (iii) screening-level analyses of sensitivity to potential climate change (iv) low-dimensional modeling where there are limited data or computation resources or technical expertise.

Acknowledgements

The research was funded through New Zealand's Foundation for Research Science and Technology, under contract C01X0304 "Land

Use Intensification: Sustainable Management of Water Quality and Quantity". The SNOTEL data was made available through the Natural Resources Conservation Service of the United States Department of Agriculture – the helpful advice and continuing quality assurance work of NRCS staff is greatly valued. Noemie Patz of Freiburg University helped develop data analysis routines. The helpful comments and advice of many colleagues are gratefully acknowledged, including David Tarboton, David Rupp, Martyn Clark, Agate Ponder-Sutton, Drew Slater, Alberto Viglione and Francesco Laio on previous versions of the manuscript.

Appendix A. Difference between two cosines

We wish to express the difference of two cosine functions (offset by some fixed phase angle, and with different amplitudes) as a third cosine function (with a different amplitude and phase). We write this difference of cosines as a cosine function, i.e.,

$$a\cos(z-\alpha) - b\cos(z-\beta) = c\cos(z-\gamma), \tag{25}$$

where c and γ are to be determined for any given values of a, α, b and β. Expanding on Potter [18], we write the cosines of differences as

$$c_1\cos(z) + c_2\sin(z) = [c\cos(\gamma)]\cos(z) + [c\sin(\gamma)]\sin(z), \tag{26}$$

with

$$c_1 = a\cos(\alpha) - b\cos(\beta), \quad c_2 = a\sin(\alpha) - b\sin(\beta). \tag{27}$$

Since $\sin(z)$ and $\cos(z)$ are linearly independent, it follows that

$$c\cos(\gamma) = c_1, \quad c\sin(\gamma) = c_2. \tag{28}$$

From Eq. (28), two results follow. First

$$c = \pm\sqrt{c_1^2 + c_2^2} = \pm\sqrt{a^2 + b^2 - 2ab\cos(\alpha-\beta)}. \tag{29}$$

Eq. (28) also implies that

$$\gamma = \tan^{-1}(c_2/c_1). \tag{30}$$

Note that by definition of the arctangent function, $-\pi/2 \leqslant \gamma \leqslant \pi/2$, and so $\cos(\gamma) \geqslant 0$. If we now substitute $z = \gamma$ in Eq. (26), we obtain

$$c = c_1\cos(\gamma) + c_2\sin(\gamma) = \cos(\gamma)[(c_1^2 + c_2^2)/c_1] \tag{31}$$

from which it follows that $\mathrm{sgn}(c_1) = \mathrm{sgn}(c)$. We now have our final result,

$$\begin{aligned} &a\cos(z-\alpha) - b\cos(z-\beta) = c\cos(z-\gamma), \quad \text{where} \\ &c = \mathrm{sgn}(c_1)\sqrt{c_1^2 + c_2^2} = \mathrm{sgn}(c_1)\sqrt{a^2 + b^2 - 2ab\cos(\alpha-\beta)}, \\ &\gamma = \tan^{-1}(c_2/c_1) = \sin^{-1}(c_2/c) \end{aligned} \tag{32}$$

and c_1 and c_2 are given in Eq. (27). The arcsine is preferred over the arctangent for practical calculation using Eq. (32) since the arcsine can be computed when $c_1 = 0$.

Appendix B. Snow accumulation period

The result of Appendix A can be used to simplify Eq. (12), by setting $z = 2\pi(t_e - s_P)/\tau, a = 1, \alpha = 0, b = 1$, and $\beta = 2\pi(t_e - t_s)/\tau$ in Eq. (32). First, we have from Eq. (27) that

$$c_1 = 1 - \cos(\beta), \quad c_2 = -\sin(\beta). \tag{33}$$

When $\beta = 2\pi(t_e - t_s)/\tau$, we obtain from Eq. (11)

$$\cos(\beta) = -\cos(2\sin^{-1}(\overline{T}^*)) = 1 - 2(1-\overline{T}^{*2}) = 2\overline{T}^{*2} - 1 \tag{34}$$

and also

$$\begin{aligned} \sin(\beta) &= \sin(2\sin^{-1}(\overline{T}^*)) = 2\sin(\sin^{-1}(\overline{T}^*))\cos(\sin^{-1}(\overline{T}^*)) \\ &= 2\overline{T}^*\sqrt{1-\overline{T}^{*2}}. \end{aligned} \tag{35}$$

Thus we have

$$\begin{aligned} &c_1 = 2(1-\overline{T}^{*2}), \quad c_2 = -2\overline{T}^*\sqrt{1-\overline{T}^{*2}}, \\ &c_1^2 + c_2^2 = 2\sqrt{1-\overline{T}^{*2}}. \end{aligned} \tag{36}$$

Since $\sin^{-1}(\overline{T}^*)$ is only defined for $-1 \leqslant \overline{T}^* \leqslant 1$, it follows that $\mathrm{sgn}(c_1) = 1$, and so

$$\gamma = \sin^{-1}(-\overline{T}^*) = -\sin^{-1}(\overline{T}^*), \tag{37}$$

We now have (using Eq. (10) for t_e)

$$z - \gamma = \frac{2\pi}{\tau}\left(t_e - s_P + \sin^{-1}(\overline{T}^*)\frac{\tau}{2\pi}\right) = \pi + \pi I(\Delta_T > 0) - \frac{2\pi s_P}{\tau}. \tag{38}$$

This gives us

$$\cos(z-\gamma) = \mathrm{sgn}(\Delta_T)\cos(2\pi s_P/\tau), \tag{39}$$

which now allows us to derive the final result

$$c\cos(z-\gamma) = 2\sqrt{1-\overline{T}^{*2}}\cos(2\pi s_P/\tau)\mathrm{sgn}(\Delta_T). \tag{40}$$

Appendix C. Definition of symbols

Symbol	Definition	Typical units
f_s	Fraction of precipitation which falls as snow	–
$g(\overline{T}^*)$	Effect of scaled temperature on potential melt	–
K	Melt factor	mm d^{-1} °C^{-1}
L	Lapse rate of temperature with elevation	°C km^{-1}
N	Lapse rate of precipitation with elevation	m y^{-1} km^{-1}
$\overline{P}$	Mean precipitation rate	mm d^{-1}
$P(t)$	Precipitation rate at time t	mm d^{-1}
$\overline{P}^*$	Dimensionless mean precipitation rate	–
P_c	Winter precipitation threshold	mm d^{-1}
$PM(t_1,t_2)$	Potential melt between times t_1 and t_2	mm
s_P	Phase shift of precipitation rate	d
s_T	Phase shift of temperature	d
t	Time	Days since origin
t_s	Time at start of snowfall	Days since origin
t_e	Time at end of snowfall	Days since origin
t_m	Time at end of snowmelt	Days since origin
$t_{coldest}$	Time of coldest temperature	Days since origin
$\overline{T}$	Mean temperature	°C
$\overline{T}^*$	Dimensionless mean temperature	–
$T(t)$	Temperature at time t	°C
T_0	Threshold temperature	°C
T_c	Winter temperature threshold	°C
W_s	Snow water equivalent storage	mm
W_s^*	Scaled snow water equivalent storage	–
δ_P	Amplitude of precipitation rate	–
Δ_T	Amplitude of temperature	°C
δ_P^*	Dimensionless amplitude of precipitation rate, taking account of phase differences between temperature and precipitation	–
τ	Duration of annual cycle	d

References

[1] Bowling LC, Pomeroy JW, Lettenmaier DP. Parameterization of blowing-snow sublimation in a macroscale hydrology model. J Hydrometeorol 2004;5(5):745–62.

[2] Cayan DR, Kammerdiener SA, Dettinger MD, Caprio JM, Peterson DH. Changes in the onset of spring in the Western United States. Bull Am Meteorol Soc 2001;82(3):399–415.
[3] Clark MP, Hendrikx J, Slater AG, Hreinsson EÖ, Kerr T, Owens IF, et al. Use of field data to design distributed snow models. Water Res Res, submitted for publication.
[4] Etchevers P, Martin E, Brown R, Fierz C, Lejeune Y, Bazile E, et al. Validation of the energy budget of an alpine snowpack simulated by several snow models (SnowMIP project). Ann Glaciol 2004;38:150–8.
[5] Hamlet AF, Mote PW, Clark MP, Lettenmaier DP. Effects of temperature and precipitation variability on snowpack trends in the Western United States. J Clim 2005;18(21):4545–61.
[6] Hantel M, Hirtl-Wielke L-M. Sensitivity of Alpine snow cover to European temperature. Int J Clim 2007;27(10):1265–75.
[7] Hock R. Temperature index melt modelling in mountain areas. J Hydrol 2003;282(1–4):104–15.
[8] Hood E, Williams M, Cline D. Sublimation from a seasonal snowpack at a continental, mid-latitude alpine site. Hydrol Process 1999;13(12–13):1781–97.
[9] Lundberg A, Koivusalo H. Estimating winter evaporation in boreal forests with operational snow course data. Hydrol Process 2003;17(8):1479–93.
[10] Lundberg A, Nakai Y, Thunehed H, Halldin S. Snow accumulation in forests from ground and remote-sensing data. Hydrol Process 2004;18(10):1941–55.
[11] Milly PCD. Climate, interseasonal storage of soil water, and the annual water balance. Adv Water Resour 1994;17:19–24.
[12] Milly PCD. Climate, soil water storage and the average annual water balance. Water Resour Res 1994;30(7):2143–56.
[13] Ohmura A. Physical basis for the temperature-based melt-index method. J Appl Meteorol 2001;40(4):753–61.
[14] Peel MC, Finlayson BL, McMahon TA. Updated world map of the Köppen–Geiger climate classification. Hydrol Earth Syst Sci 2007;11(5):1633–44.
[15] Perona P, Porporato A, Ridolfi L. A stochastic process for the interannual snow storage and melting dynamics. J Geophys Res 2007;112:D08107.
[16] Pomeroy JW, Essery RLH. Turbulent fluxes during blowing snow: field tests of model sublimation predictions. Hydrol Process 1999;13(18):2963–75.
[17] Pomeroy JW, Gray DM, Hedstrom NR, Janowicz JR. Prediction of seasonal snow accumulation in cold climate forests. Hydrol Process 2002;16(18):3543–58.
[18] Potter NJ. Statistical–dynamical modelling of catchment water balance: climatic and vegetation controls on hydrologic fluxes. The University of Melbourne, Parkville, Victoria, Australia, Melbourne; 2006. 305 p.
[19] Potter NJ, Zhang L, Milly PCD, McMahon TA, Jakeman AJ. Effects of rainfall seasonality and soil moisture capacity on mean annual water balance for Australian catchments. Water Resour Res 2005;41:W06007.
[20] Serreze MC, Clark MP, Armstrong RL, McGinnis DA, Pulwarty RS. Characteristics of the western United States snowpack telemetry (SNOTEL) data. Water Resour Res 1999;35(7):2145.
[21] Shulski MD, Seeley MW. Application of snowfall and wind statistics to snow transport modeling for snowdrift control in Minnesota. J Appl Meteorol 2004;43(11):1711–21.
[22] Slater AG, Schlosser CA, Desborough CE, Pitman AJ, Henderson-Sellers A, Robock A, et al. The representation of snow in land surface schemes: results from PILPS 2(d). J Hydrometeorol 2001;2(1):7–25.
[23] Sturm M, Holmgren J, Liston GE. A seasonal snow cover classification-system for local to global applications. J Clim 1995;8(5):1261–83.
[24] Tabler RD. Controlling blowing and drifting snow with snow fences and road design. National Cooperative Highway Research Program Project No. 20-7(147), 2003. 346 p.
[25] Woods RA. The relative roles of climate, soil, vegetation and topography in determining seasonal and long-term catchment dynamics. Adv Water Resour 2003;26(3):295–309.
[26] Yang Z-L, Dickinson RE, Robock A, Vinnikov KY. Validation of the snow submodel of the biosphere atmosphere transfer scheme with russian snow cover and meteorological observational data. J Clim 1997;10(2):353–73.